Atmospheric pressure change associated with the 2003 Tokachi-Oki earthquake

Shingo Watada,[1] Takashi Kunugi,[2] Kenji Hirata,[3] Hiroko Sugioka,[3] Kiwamu Nishida,[1] Shoji Sekiguchi,[2] Jun Oikawa,[1] Yoshinobu Tsuji,[1] and Hiroo Kanamori[4]

Received 1 September 2006; revised 10 November 2006; accepted 15 November 2006; published 21 December 2006

[1] Clear atmospheric pressure changes associated with the 2003 Tokachi-Oki, Japan, earthquake with Mw 8.3 were recorded with the microbarographs distributed in Japan. The pressure change starts at the arrival of seismic waves and reaches its maximum amplitude at the arrival of Rayleigh waves, suggesting that the observed pressure change was driven by the ground motion of seismic waves passing by the site. We computed the seismic-to-pressure transfer function (i.e., the spectral ratio of the pressure change to the vertical ground motion velocity) for periods between 10 to 50 s from the co-located barograph and seismograph records. Comparison of the observed transfer function with the theoretical one including the finite frequency and wavelength effects for a gravitationally stratified isothermal atmosphere confirms that the observed amplitude and phase of the pressure change are explained by the acoustic coupling between the atmosphere and the ground just beneath the sensors. **Citation:** Watada, S., T. Kunugi, K. Hirata, H. Sugioka, K. Nishida, S. Sekiguchi, J. Oikawa, Y. Tsuji, and H. Kanamori (2006), Atmospheric pressure change associated with the 2003 Tokachi-Oki earthquake, *Geophys. Res. Lett.*, *33*, L24306, doi:10.1029/2006GL027967.

1. Introduction

[2] The pressure changes after large earthquakes have been reported and three types of pressure sources are identified. For the 1964 Alaskan earthquake, *Donn and Posmentier* [1964] showed that the vertical ground motion of traveling Rayleigh waves at the pressure recording site caused pressure changes. *Mikumo* [1968] successfully modeled the air waves originated from the subsidence or uplift in the earthquake source area by introducing a finiteness of the source. *Young and Greene* [1982] provided evidence from a few microphone arrays in North America that air waves were radiated from the Rocky Mountains at the arrival of seismic Rayleigh waves.

[3] Recent development of IMS microphone arrays, a part of the International Monitoring System (IMS), generated a rush of infrasound data analysis after the 2001 Arequipa, Peru, earthquake [*Le Pichon et al.*, 2002], the 2001, Kunlun, China, earthquake [*Le Pichon et al.*, 2003], the 2002 Denali, Alaska, earthquake [*Olson et al.*, 2003], the 2003 Tokachi-Oki, Japan, earthquake [*Kim et al.*, 2004], and the 2004–2005 Sumatra earthquakes [*Le Pichon et al.*, 2005].

[4] The Tokachi-Oki earthquake is unique in that the spatial and temporal propagation of co-seismic ionospheric disturbance (CID) is observed by a dense Global Positioning System array in Japan [*Heki and Ping*, 2005]. Heki and Ping reported that the CID traveled at the speed of sound, about 1 km/sec, in the ionosphere. However, no CID at the speed of Rayleigh waves was observed. In contrast, *Ducic et al.* [2003] reported that CID traveling at the speed of Rayleigh waves was identified at teleseismic distance.

[5] The surface deformation in the epicentral area [*Calais and Minster*, 1995] and traveling Rayleigh waves [*Ducic et al.*, 2003] have been identified as the origins of ionospheric disturbance. A numerical modeling of the development of ionospheric disturbance from traveling surface waves has been proposed [*Artru et al.*, 2004].

[6] In this paper we directly measure the pressure disturbance and the ground motion during the passage of large amplitude Rayleigh waves of the Tokachi-Oki earthquake with co-located microbarographs and broadband seismometers, and compare the observation with theoretical transfer functions. Since the missing CID traveling at the Rayleigh wave speed remains a puzzle, we hope that our results will provide a definitive initial wavefield for ionospheric studies.

2. Observation

[7] Quartz pressure-transducer type microbarographs capable of recording the absolute atmospheric pressure with a resolution of 0.2 Pa at 1 Hz sampling rate are distributed in Japan (Figure 1 and Table 1) and recorded pressure fluctuation during the 2003 Tokachi-Oki earthquake (Figure 2). Microbarographs and co-located broadband seismometers recorded waves with a dominant period of about 15–20 s for more than 20 min. The seismic and pressure disturbances traveled through Japan at a constant velocity of about 3.2 km/s with a maximum amplitude of about a few mm/s and a few Pascal, respectively (Figure 3). The waveforms of the vertical ground velocity and high-pass filtered pressure changes are very similar (Figure 4); this suggests that the pressure disturbance is generated locally by the vertical ground motion of traveling Rayleigh waves. On our microbarograms at two sites, we have detected a pressure fluctuation which can be interpreted as air waves generated at the earthquake source region and propagated at a speed of about 260 m/s but at other sites the pressure signal is not as clear as the ground-coupled Rayleigh waves are.

[1] Earthquake Research Institute, University of Tokyo, Tokyo, Japan.
[2] National Research Institute for Earth Science and Disaster Prevention, Ibaraki, Japan.
[3] Japan Agency for Marine-Earth Science and Technology, Kanagawa, Japan.
[4] Seismological Laboratory, California Institute of Technology, Pasadena, California, USA.

0094-8276/06/2006GL027967

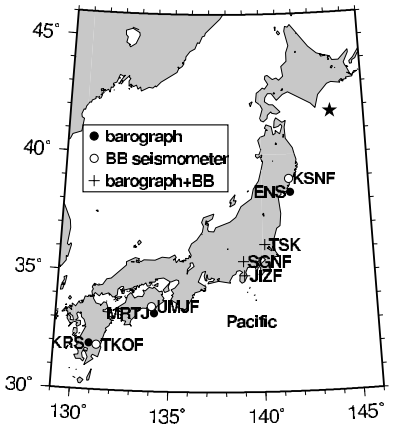

Figure 1. Station map. Star denotes the epicenter of the M = 8.3 2003 Tokachi-Oki earthquake which occurred on September 25, 2003, 19:50 (UT). Filled circles, circles, and plus symbols denote the barograph, broadband seismometer, and co-located barograph and broadband seismometer, respectively.

[8] A barograph is mechanically sensitive to the motion of itself, and a barograph placed on the ground is also sensitive to the ground motion [*Bedard*, 1971]. We have tested the mechanical sensitivity of the quartz-type microbarographs placed on a shake table and confirmed that, at a period of 10 s or longer, the microbarograph is not affected by the ground motion with a vertical and horizontal velocity of less than 1 cm/s [*Watada and Ohminato*, 2006].

[9] The effect of wind noise is reduced for microbarographs placed in the vault of broadband seismometers. No phase lag between the barometers inside and outside the vault was detected because the pressure inside of the vault is quickly equilibrated with the pressure outside through drainage.

3. Acoustic Coupling Between the Atmosphere and the Solid Earth

[10] Generation of atmospheric disturbance by ground motion is often modeled by a simple relationship between the ground velocity and the pressure change at the surface with an assumption that the time scale of the vertical motion is short compared with the acoustic cut-off period. Excess pressure in a homogeneous fluid medium caused by the vertical motion is given by, e.g., *Lighthill* [1978],

$$p' = \rho c_s w, \tag{1}$$

where p', ρ, c_s, and w denote the excess pressure, air density, sound velocity, and velocity of fluid motion, respectively. As the wave frequency becomes close to the acoustic cut-off frequency in the gravitationally stratified atmosphere, and the wavelength approaches the scale height of the atmosphere, the relation between p' and w deviates from equation (1).

3.1. Measurement of Transfer Function

[11] The seismic-pressure transfer function is defined by the spectral ratio of the pressure perturbation above the ground to the ground surface vertical velocity as a function of frequency and horizontal wavelength. We computed the transfer function from the pressure and the velocity records containing the peak of Rayleigh waves at JIZF. Figure 5 shows the amplitude ratio and the phase difference. At a frequency of 0.02 Hz or higher, the amplitude ratio and phase difference are nearly constant, which is consistent with equation (1). At a frequency of 0.02 Hz or lower, the atmospheric pressure data is dominated by the background noise and accurate amplitude and phase measurements become difficult.

[12] *Kim et al.* [2004] observed air waves generated near the source region of the Tokachi-Oki earthquake and traveled as sound waves in the atmosphere as well as those locally generated by Rayleigh waves at two seismo-acoustic arrays in Korea. The amplitude transfer function was estimated from the co-located seismic broadband instruments and infrasound sensors. They found that the observed seismic to infrasound transfer function is flat from 0.03 to 1.0 Hz. The estimated amplitude data of the transfer function at each sensor of an infrasound array show a scatter in the period range longer than about 30 sec, similar to our measurement.

[13] Our results complement *Kim et al.*'s [2004] results. In addition to the amplitude spectrum, we measured the phase spectrum and found no phase difference between the ground velocity and pressure, confirming that the observation is consistent with equation (1).

3.2. Theoretical Transfer Function

[14] We investigate the acoustic coupling between long-period acoustic waves in the atmosphere and ground mo-

Table 1. Instrument Locations and Types[a]

Site	Sensor Type	Latitude, degree	Longitude, degree	Epicentral Distance, km
Sugeno, SGNF	MB[b], STS-1	35.5044	138.9475	827
Nakaizu, JIZF	MB[b], STS-1	34.9129	138.9972	882
Tsukuba, TSK	MB[b], STS-1	36.2098	140.1104	707
Enoshima, ENS	MB[c]	38.4001	141.5963	431
Kesennuma, KSNF	STS-2	38.9733	141.5333	379
Muroto, MRTJ	MB[c]	33.2977	134.1882	1283
Umaji, UMJF	STS-2	33.5054	134.0398	1269
Kirishima, KRS	MB[c]	31.9441	130.8418	1604
Takaoka, TKOF	STS-2	31.8894	131.2347	1583

[a]MB stands for a microbarograph which measures the absolute atmospheric pressure change with a resolution of 0.2 Pascal at every 1 sec. STS-1 and STS-2 stand for broadband seismometers with a cutoff corner frequency at 360 and 120 sec, respectively.
[b]Microbarograph APDL-1000S. See *Nishida et al.* [2005] for the sensor specification.
[c]Microbarograph Proscientific model 760-16B. See *Watada and Kunugi* [2000] for system configuraton. Both APDL-1000S and 760-16B use a Paroscientific 216B pressure-transducer inside.

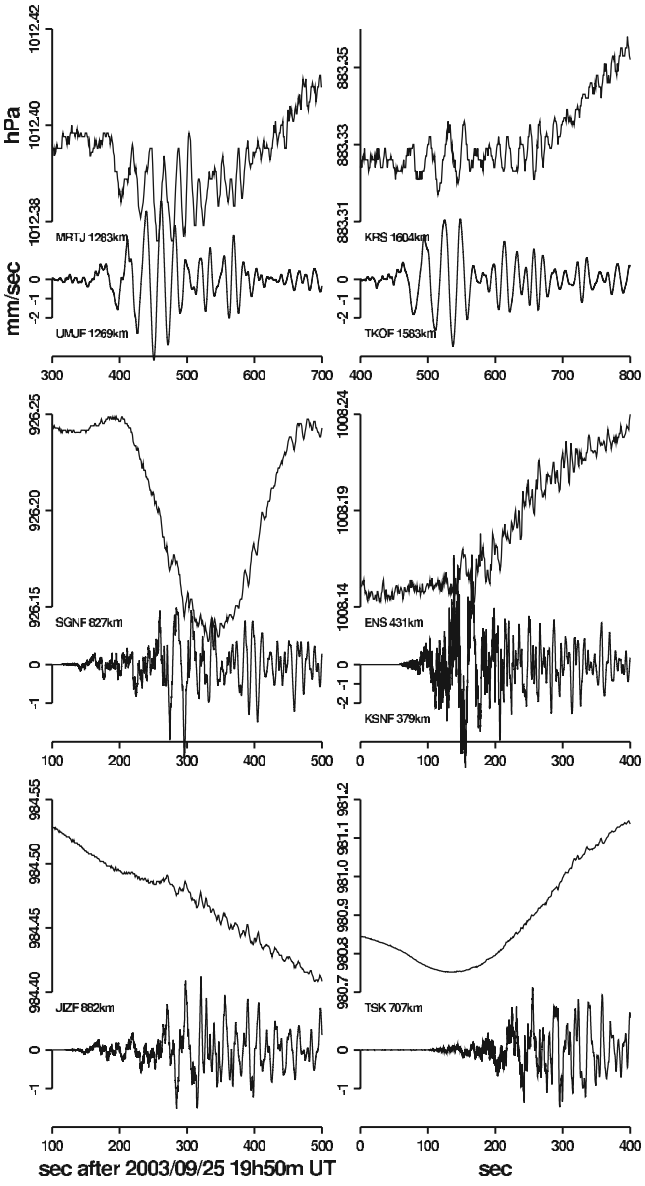

Figure 2. Comparison of the original barograms and the vertical-component seismograms during the arrival of Rayleigh waves observed at co-located (SGNF, JIZF, TSK) and nearby stations (MRTJ-UMJF, KRS-TKOF, ENS-KSNF). Note that the pressure records give the absolute atmospheric pressure. Offset of the absolute pressure indicates the difference in altitude of the sites. Long-period undulations in the microbarograms are the background atmospheric pressure variations. At nearby stations, the phase between the ground velocity and atmospheric pressure is not the same, because of the small difference in the epicentral distances. A 10 km difference will result in about 3 sec time shift.

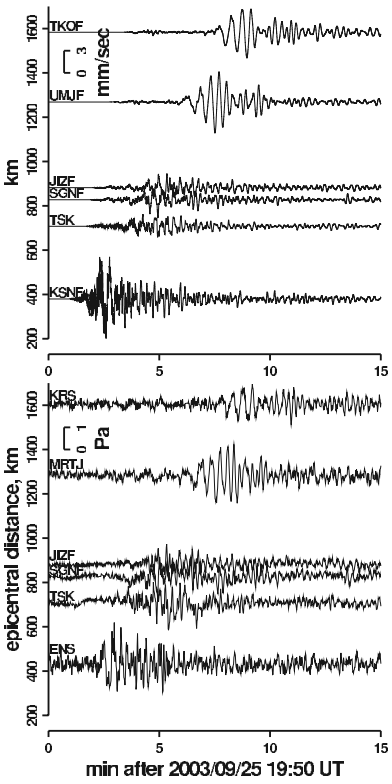

Figure 3. (top) Record section of the vertical-component velocity seismograms compared with (bottom) that of atmospheric pressure changes high pass filtered for 50 s and shorter periods.

tion. We assume an isothermal atmosphere underlain by a flat horizontal ground in which seismic waves propagate. *Mikumo* [1968] examined a more realistic atmospheric model accounting for a finite frequency but infinite wavelength to model the ground-atmosphere coupling induced by a large permanent deformation over a wide source region. In this section, we derive the transfer function for the ground-atmosphere coupling as a function of frequency and horizontal wave number. Following *Gill* [1982, p. 171], we take the positive z and x axes along the vertical upward and horizontal directions, respectively. We consider 1-D plane waves propagating parallel to the x-z plane, hence

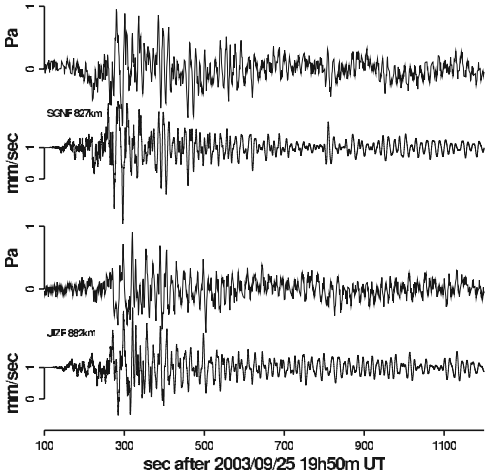

Figure 4. Comparison of the high pass filtered microbarograms for the period of 50 s and shorter and original seismograms at two co-located sites. Upper pair is at SGNF and the lower pair is at JIZF. In each pair, top trace is a high-pass filtered microbarogram, and bottom trace is the original vertical component seismogram. High-pass filtered microbarograms and vertical ground motions show striking similarity for the first 20 minutes from the beginning.

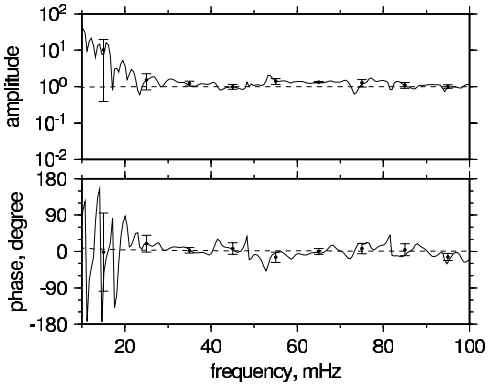

Figure 5. The seismic-pressure transfer function at JIZF where we have the most stable estimate, (top) amplitude and (bottom) phase. The transfer function is computed by spectral division of the pressure record by the velocity seismograms. 10 minute time windows starting at 19:50 UT are used. Horizontal dashed lines indicate the theoretical values from equation (4) with $\rho_0 = 1.225$ kg/m^3 and $c_s =$ 331 m/s of the standard atmosphere model. Average values and standard deviations of each 0.01 Hz bin are also plotted with an error bar.

dependence on the y-coordinate is dropped. The scaled pressure $P = \rho_0^{-1/2} p'$ and vertical velocity $W = \rho_0^{1/2} w$, where ρ_0, p', and w are the background air density, the Eulerian pressure perturbation, and vertical upward velocity, respectively, have plane wave solutions with a common angular frequency and wavenumber in the form exp $i(kx + mz - \omega t)$. We need not use the cylindrical coordinates because the seismic and barograph stations are located more than 400 km away from the epicenter, much larger than the wavelength of seismic surface waves and air waves we analyze in this study.

[15] The dispersion relation of air waves is expressed in the form [*Gill*, 1982, p.172]

$$c_s^{-2}\omega^4 - \omega^2\left(k^2 + m^2 + N^2/c_s^2 + \Gamma^2\right) + k^2N^2 = 0 \qquad (2)$$

where Γ and the buoyancy frequency N are defined by equation 6.14.19, and equation 6.14.4 in *Gill* [1982], respectively. Using ω_a, the acoustic cut-off frequency defined by *Houghton* [1986, equation (8.22)], this can be also written as [*Houghton*, 1986, p.108]

$$m^2 = k^2\left(\frac{N^2}{\omega^2} - 1\right) + \frac{\omega^2 - \omega_a^2}{c_s^2}. \qquad (3)$$

Then the seismic-pressure transfer function normalized by air density and sound velocity can be derived using equations 6.14.17–18 from *Gill* [1982] and equations (2) or (3) as

$$\frac{p'}{\rho_0 c_s w} = \frac{P}{c_s W} = \frac{\omega/\omega_a}{\left(\frac{\omega^2}{\omega_a^2} - 4k^2H^2\right)}\left(2D(m)H + i\frac{2-\gamma}{\gamma}\right), \qquad (4)$$

where $D(m) \equiv \sqrt{m^2}$ for $m^2 \geq 0$ and $D(m) \equiv i\sqrt{-m^2}$ for $m^2 < 0$, corresponding to propagating waves and evanescent waves in the vertical direction, respectively, γ is the ratio of specific heat of dry air, H is a scale height given by $H = c_s^2/\gamma g$, and g is the gravity acceleration.

[16] For large frequency and horizontal wave number, equation (4) is reduced to a simple form

$$\frac{p'}{\rho_0 c_s w} = \frac{1}{\sqrt{1 - \left(\frac{c_s}{\omega/k}\right)^2}}. \qquad (5)$$

For a diatomic gas, $\gamma = 1.4$. If we adopt $H = 8.0$ km, $g =$ 9.8 m/s^2, then sound velocity $c_s = 331.3$ m/s, acoustic cut-off frequency $\omega_a = 0.0207$ rad/s, cut-off period $2\pi/\omega_a =$ 303.4 s, buoyancy frequency $N = 0.0187$ rad/s, and the buoyancy period $2\pi/N = 335.9$ s. Figure 6 shows the right-hand side of equation (4) as a function of the scaled frequency, ω/ω_a, with the horizontal phase velocity ω/k as a parameter.

[17] The transfer function for the purely vertically propagating wave (i.e., $\omega/k = \infty$) deviates from the simple relation equation (1) at frequencies lower than 6 ω/ω_a. The amplitude ratio diminishes and the phase of the air wave advances. For a finite horizontal wavelength corresponding to a phase velocity of the Rayleigh waves of the Tokachi-Oki earthquake both the amplitude ratio and phase difference are nearly identical to those of the purely vertically propagating waves. With a lower phase velocity close to the sound velocity in the air, the amplitude ratio and phase difference start to deviate from those of the purely vertical propagation.

4. Conclusion and Discussion

[18] We determined the seismic-pressure transfer function from the seismograms and pressure records of the Tokachi-Oki earthquake recorded with co-located instruments. The phase and amplitude of the observed transfer function are nearly constant over the period from 10 s ($\omega/\omega_a = 30$) to 50 s ($\omega/\omega_a = 6$) (Figure 5). The constant phase value is close to zero and the constant amplitude value is approximately $\rho_0 c$ as predicted by equation (1) because the phase velocity

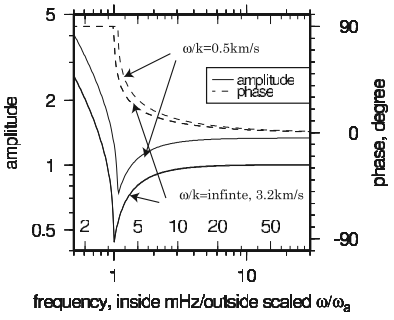

Figure 6. Theoretical transfer functions for an isothermal atmosphere including the effect of the finite period and finite horizontal wavelength, as expressed in equation (4). Dashed and solid curves denote phase and amplitude transfer functions, respectively. $\omega/k =$ infinite corresponds to the purely vertical propagation with infinite horizontal wavelength. 3.2 km/s corresponds to the phase speed of seismic Rayleigh waves. The curves for the cases of 3.2 km/s and infinite km/s nearly coincide on the plot.

of the Rayleigh waves is one order of magnitude larger than the sound velocity in the air and equation (5) is close to one. The theoretical transfer function indicates that the simple pressure-velocity relationship given by equation (1) is valid for the frequency band and horizontal wavelength of seismic Rayleigh waves. At periods longer than 50 s ($\omega/\omega_a < 6$), the theory predicts that the phase will increase and the amplitude will decrease. Unfortunately, we cannot confirm this behavior with our data. The Fourier amplitude spectrum of our pressure record is inversely proportional to frequency which is similar to that of the background atmospheric pressure data [*Nishida et al.*, 2005]; this suggests that the noise level of our pressure data at period longer than 50 s is higher than the ground-coupled acoustic waves.

[19] The waveforms of the ground velocity and the pressure fluctuation are very similar for at least 20 minutes after the arrival of seismic waves (Figure 4). The transfer function computed from the later part of the data is not as constant as the one computed from the first 10 minute data. The lesser stability of the transfer function from the later part of the data is partly because of the low S/N due to the smaller ground velocity, and because the scattered atmospheric waves generated at and propagated from distant locations enter the atmosphere near the barometers.

[20] The mechanism of the missing CID at the speed of Rayleigh waves for the 2003 Tokachi-Oki earthquake is not clear. Our ground pressure measurements confirmed that coherent air waves were generated from the traveling Rayleigh waves at the surface, as theory predicts. Thus, the cause of the missing CID must be sought in the mechanism of atmospheric wave propagation from the lower atmosphere to ionosphere in the epicentral area.

[21] **Acknowledgments.** We thank M. Koyama, F. Masutani, and Y. Yanagawa for barometer station operations, and Y. Fukao for instrumentation. Discussions with T. Sakai, M. Tahira and T. Mikumo were useful. This research is partially supported by the Ministry of Education, Science, Sports and Culture, Grant in Aid for Scientific Research (C), 15540404 and 18540413.

References

Artru, J., T. Farges, and P. Lognonné (2004), Acoustic waves generated from seismic surface waves: Propagation properties determined from Doppler sounding observations and normal-mode modeling, *Geophys. J. Int.*, *158*, 1067–1077.

Bedard, A. J. (1971), Seismic response of infrasound microphones, *J. Res. Natl. Bur. Stand. U.S., Sect. C*, *75*, 41–45.

Calais, E., and J. B. Minster (1995), GPS detection of ionospheric perturbations following the January 17, 1994, Northridge earthquake, *Geophys. Res. Lett.*, *22*, 1045–1048.

Donn, W. L., and E. S. Posmentier (1964), Ground-coupled air waves from the great Alaskan earthquake, *J. Geophys. Res.*, *69*, 5357–5361.

Ducic, V., J. Artru, and P. Lognonné (2003), Ionospheric remote sensing of the Denali Earthquake Rayleigh surface waves, *Geophys. Res. Lett.*, *30*(18), 1951, doi:10.1029/2003GL017812.

Gill, A. E. (1982), *Atmosphere-Ocean Dynamics*, Elsevier, New York.

Heki, K., and J. Ping (2005), Directivity and apparent velocity of the coseismic ionospheric disturbances observed with a dense GPS array, *Earth Planet. Sci. Lett.*, *236*, 845–855.

Houghton, J. T. (1986), *The Physics of Atmospheres*, 2nd ed., 271 pp., Cambridge Univ. Press, New York.

Kim, T. S., C. Hayward, and B. Stump (2004), Local infrasound signals from the Tokachi-Oki earthquake, *Geophys. Res. Lett.*, *31*, L20605, doi:10.1029/2004GL021178.

Le Pichon, A., J. Guilbert, A. Vega, M. Garcés, and N. Brachet (2002), Ground-coupled air waves and diffracted infrasound from the Arequipa earthquake of June 23, 2001, *Geophys. Res. Lett.*, *29*(18), 1886, doi:10.1029/2002GL015052.

Le Pichon, A., J. Guilbert, M. Vallée, J. X. Dessa, and M. Ulziibat (2003), Infrasonic imaging of the Kunlun Mountains for the great 2001 China earthquake, *Geophys. Res. Lett.*, *30*(15), 1814, doi:10.1029/2003GL017581.

Le Pichon, A., P. Herry, P. Mialle, J. Vergoz, N. Brachet, M. Garcés, D. Drob, and L. Ceranna (2005), Infrasound associated with 2004–2005 large Sumatra earthquakes and tsunami, *Geophys. Res. Lett.*, *32*, L19802, doi:10.1029/2005GL023893.

Lighthill, J. (1978), *Waves in Fluids*, Cambridge Univ. Press, New York.

Mikumo, T. (1968), Atmospheric pressure waves and tectonic deformation associated with the Alaskan earthquake of March 28, 1964, *J. Geophys. Res.*, *73*, 2009–2025.

Nishida, K., Y. Fukao, S. Watada, N. Kobayashi, M. Tahira, N. Suda, N. Nawa, T. Oi, and T. Kitajima (2005), Array observation of background atmospheric waves in the seismic band from 1mHz to 5mHz, *Geophys. J. Int.*, *162*, 824–840.

Olson, J. V., C. R. Wilson, and R. A. Hansen (2003), Infrasound associated with the 2002 Denali fault earthquake, Alaska, *Geophys. Res. Lett.*, *30*(23), 2195, doi:10.1029/2003GL018568.

Watada, S., and T. Kunugi (2000), Cost effective automated data collection and transmission system for microbarograph network using free-Unix, *Tech. Res. Rep. Earthq. Res. Inst., Univ. Tokyo*, *6*, 33–37.

Watada, S., and T. Ohminato (2006), Acceleration response of a barometer using shake table, *Tech. Res. Rep. Earthq. Res. Inst., Univ. Tokyo*, *12*, 19–23.

Young, J. M., and G. E. Greene (1982), Anomalous infrasound generated by the Alaskan earthquake of 28 March 1964, *J. Acoust. Soc. Am.*, *71*, 334–339.

K. Hirata and H. Sugioka, Japan Agency for Marine-Earth Science and Technology, 2-15 Natsushima-cho, Yokosuka, Kanagawa 237-0061, Japan. (hiratak@jamstec.go.jp; hikari@jamstec.go.jp)

H. Kanamori, Seismological Laboratory, California Institute of Technology, MC252-21, 1200 East California Blvd., Pasadena, CA 91125, USA. (hiroo@gps.caltech.edu)

T. Kunugi and S. Sekiguchi, National Research Institute for Earth Science and Disaster Prevention, 3-1 Tenno-dai, Tsukuba, Ibaraki 305-0006, Japan. (kunugi@bosai.go.jp; seki@bosai.go.jp)

K. Nishida, J. Oikawa, Y. Tsuji, and S. Watada, Earthquake Research Institute, University of Tokyo, 1-1-1 Yayoi Bunkyo-ku, Tokyo 113-0032, Japan. (knishida@eri.u-tokyo.ac.jp; oikawa@eri.u-tokyo.ac.jp; tsuji@eri.u-tokyo.ac.jp; watada@eri.u-tokyo.ac.jp)